Electromagnetic Characterisation of a Short-Stroke Ferromagnetic Actuator

R. M. Inston and H. Karimjee

Abstract—This experiment demonstrated the use of FEMM as an analysis tool for a short stroke ferromagnetic actuator.

I. Nomenclature

R_w, Winding resistance, $[\Omega]$

l_w, Length into the page of winding, [m]

A_w, Area of winding, $[m^2]$

V_w, Volume of winding, $[m^3]$

N, Number of turns in the winding, [-]

σ, Conductivity of winding, $[Sm^{-1}]$

k_{PF}, Packing factor of conductors in the winding, [-]

L, Inductance of the winding, [H]

$\mathcal{R}$, Reluctance, $[H^{-1}]$

A_{eff}, Effective area of air gap, $[m^2]$

W, Width of air gap, [m]

T, Thickness of air gap, [m]

g, Air gap length, [m]

II. Introduction

Finite Element Method Magnetics (FEMM) is an implementation of Finite Element Analysis (FEA) that specialises in electro-magnetics. This tool, in combination with MATLAB or another scripting language such as Python, can be used to create a series of numerical situations, from which a electro-magnetic and then mechanical analysis can be extracted.

Here, FEMM is being used to characterise a magnetic actuator, made up of an armature and a core which share the same ferromagnetic properties, two sets of windings around the top and bottom of the core and three air gaps of note, as in figure 1. This characterisation will be done analytically, neglecting and accounting for fringing, and numerically, using both a linear and non-linear ferromagnetic material.

III. Model Meshing

To perform FEA, a model is split into elements. The elements must be small enough to output an accurate enough answer despite the linearisation of the physics involved, whilst not being too small so as to increase the computational time to an unreasonable length.

FEMM has a smart-meshing tool in which the software analyses the model and allocates a dense mesh where higher resolution analysis is required and a sparse mesh where it is not. This is evident in the difference between figures 2 & 3. Although useful, this feature increases the mesh
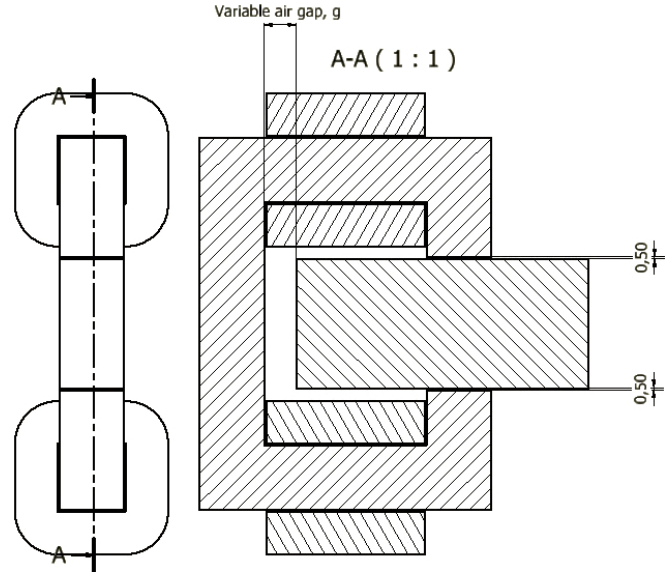

Fig. 1. Cross-sectional view of the actuator with the three air gaps higlighted (All measurements in mm).

elements (see table I) without knowing any information about the overarching aim of the problem. This is illustrated at the boundaries of the variable air gap between the movable armature and core, which is vital for the analysis of the force-displacement characteristic of the actuator. Smart-meshing fails to recognise these edges as paramount to the analysis and produces a grid seen in figure 4. By manually setting the spacing of meshing along these lines, FEMM can produce a denser, more regular mesh as seen in figure 5. This accuracy has its cost in terms of mesh elements (table I) and computational time.

Smart-meshing	Dense Air gap	Mesh Elements
OFF	OFF	14790
OFF	ON	16334
ON	OFF	22668
ON	ON	24368

TABLE I
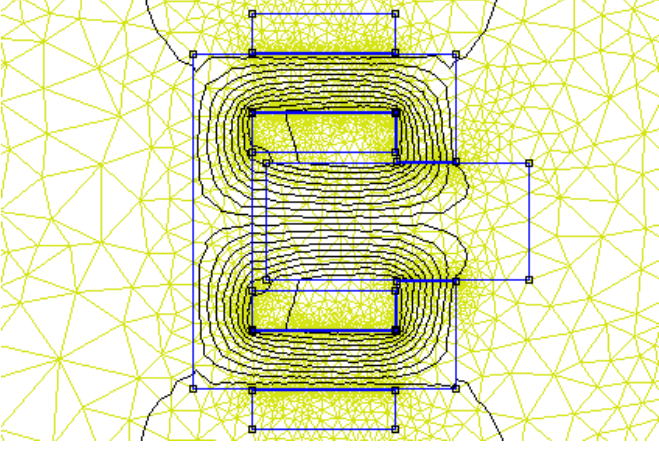A SUMMARY OF MESHING OPTIONS FOR THE MODEL.

Fig. 2. Example mesh with smart-meshing disabled. Note the sparseness of the triangulation.
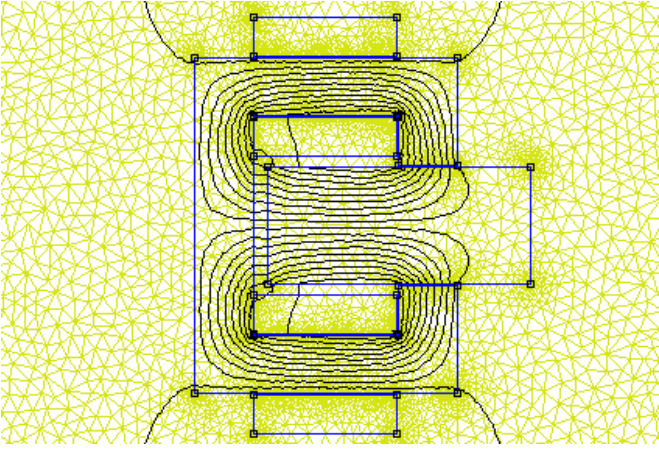

Fig. 3. Example mesh with smart meshing enabled. Note how the density increases around boundaries of interest.

IV. WINDING RESISTANCE

To calculate the winding resistance, R_w, two approaches were used: extracting resistance from FEMM and analytical. FEMM can calculate the winding resistance by obtaining the voltage and current across and through the winding respectively, and finding the resistance using Ohm's law. The analytical approach used block integrals in FEMM to obtain winding area and volume, and hence the winding depth (into the page) can be found using equation 1:

$$l_w = \frac{V_w}{A_w} \quad (1)$$

The analytical resistance is thus calculated using equation 2. The resistances of each calculation method are presented in table II.

$$R_w = \frac{N l_w}{\sigma \left(\frac{k_{PF} A_w}{N} \right)} \quad (2)$$

Table II shows a significant difference in estimated values. The analytical value uses a packing factor, $k_{PF} = 0.6$, that compensates for the space used by the insulating material in
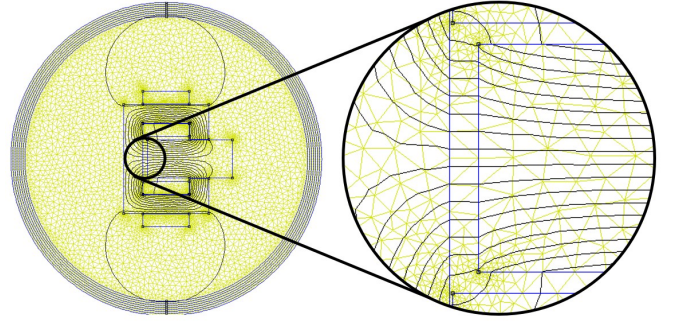

Fig. 4. FEMM smart-meshing output without specifying the area of interest. The density is low despite smart-meshing being on.
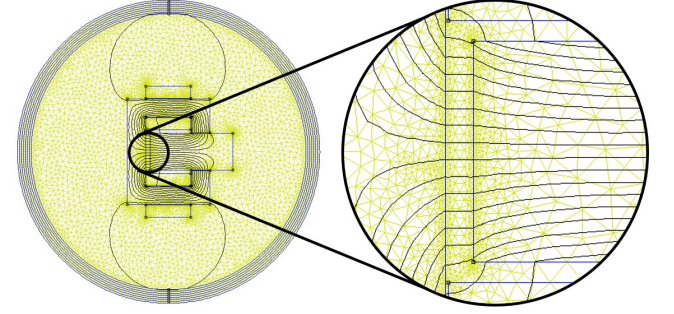

Fig. 5. FEMM smart-meshing output with specifying the area of interest and increasing the density of mesh elements within.

a winding. FEMM sees the entire area as conducting material and hence the implied cross sectional area of wire increases. Given the conductivity $\sigma = 58\text{MS/m}$ in both predictions, the greater the implied length of winding, the greater the winding resistance, R_w. However, FEMM is working with a 2D model and the analysis was performed on the top and bottom sections of the winding only. This means the analysis does not account for the whole length around the winding, notably the rounded corners and sides, causing the FEMM estimate to be at least a factor of four smaller than the analytical prediction.

Method	Current [A]	Winding Resistance [Ω]
FEMM	10	0.0107
Analytical	10	0.0557

TABLE II
A SUMMARY OF WINDING RESISTANCE CALCULATION FOR DIFFERENT METHODS.

The resistances resulting from these two methods were used to calculate the power loss through the windings for a range of current values using equation 3. This was then plotted giving the graph in figure 6. Clearly, this shows the power loss based on the analytically calculated resistance quickly becomes far greater than that of the FEMM calculated resistance. As such, if the analysis performed on the actuator were to be taken further into real applications, the analytical power loss should be considered when specifying power

dissipation requirements, rather than the FEMM output.
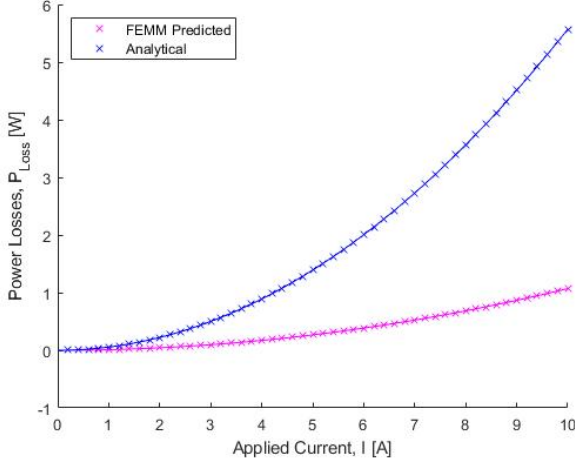
$$P_{loss} = I^2 R \qquad (3)$$

Fig. 6. Power loss against current based on equation 3 for analytical and FEMM calculated resistances. A quadratic curve produces the line of best fit.

V. WINDING INDUCTANCE

Similarly to the winding resistance, the inductance of the windings can be found analytically and numerically. To estimate the value analytically equation 4 is followed.

$$L = \frac{N^2}{\sum \mathcal{R}} \qquad (4)$$

Assuming flux is conserved, the total reluctance can be calculated based on a magnetic equivalent circuit, fig. 7. Note this is only half of the complete circuit for the actuator.

$$\sum \mathcal{R} = \mathcal{R}_{core} + \mathcal{R}_{air} + \mathcal{R}_{armature} + \mathcal{R}_{gap} \qquad (5)$$

$$\mathcal{R} = \frac{l}{\mu_0 \mu_r A} \qquad (6)$$

To improve accuracy, fringing effects can be taken into account by replacing A in equation 6 with A_{eff} from equation 7 for $\mathcal{R}_{airgap}$ and $\mathcal{R}_{variable}$.

$$A_{eff} = (W + 2g)(T + 2g) \qquad (7)$$

As only half of the equivalent circuit (shown in fig 7) was used to calculate the inductance, the result was doubled to find the total inductance for the whole actuator. To allow for this, only half of the armature and variable air gap areas was used in the original calculation.

This gives a total of two analytical values. Numerically, two values of inductance can be estimated using FEMM by using a linear or non-linear approximation of core and armature properties. The inductance varies with the displacement of the armature, evident in figure 8.
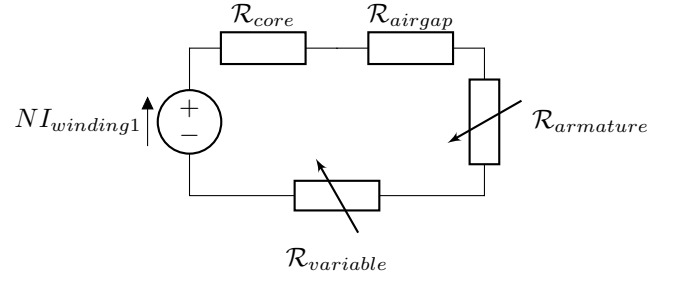

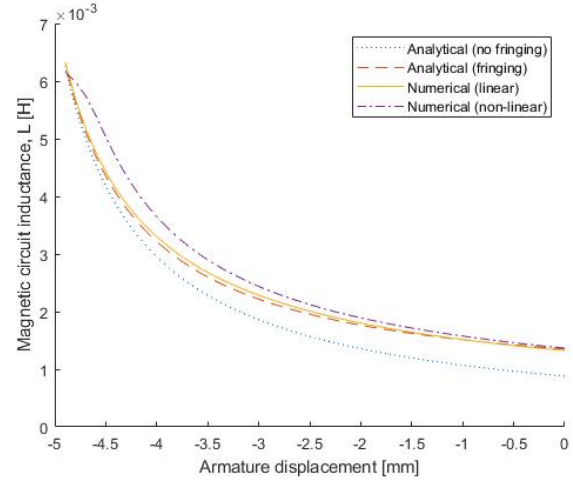Fig. 7. Half equivalent magnetic circuit for the ferromagnetic actuator.

Fig. 8. Graph showing inductance versus armature displacement for the varying methods of calculation.

VI. FORCE ON THE ARMATURE

The force on the armature of the actuator is exponentially related to its position relative to the core. As the armature approaches the core the air-gap narrows, and so the reluctance of the magnetic circuit decreases and hence the inductance of the coil increases. This allows a stronger magnetic field for a given winding current, and therefore a greater force applied to the armature.
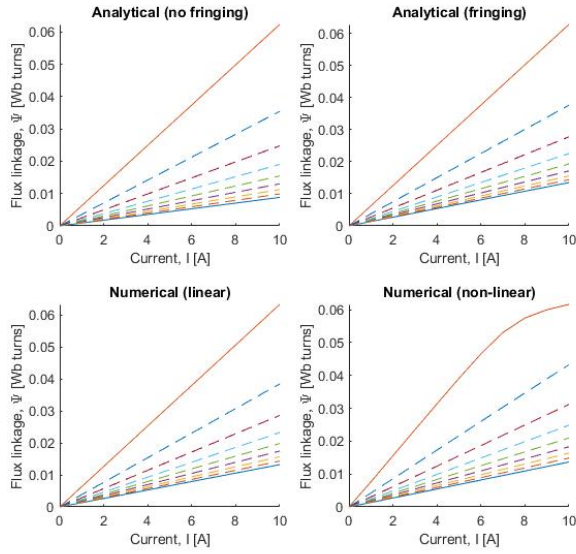
VII. CONCLUSION

Fig. 9. Ψ-I diagrams for the four methods of calculating inductance. Note saturation reached in the non-linear graph. Shown for zero displacement, maximum displacement (-49mm) and seven linearly spaced intervals between (dashed lines).
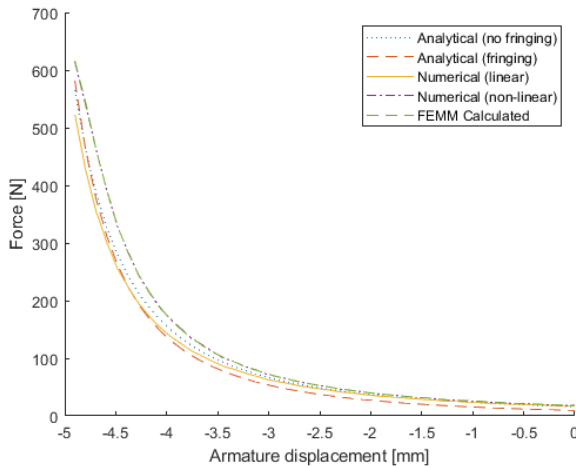
Armature Displacement [mm]	Change in Co-Energy [J]			
	Analytical (no fringing)	Analytical (fringing)	Numerical (linear)	Numerical (non-linear)
0.200	7.867	6.620	8.442	9.110
0.300	8.158	6.888	8.264	8.826
0.400	8.467	7.172	8.930	9.635
0.500	8.793	7.473	8.977	9.694
0.600	9.138	7.791	9.511	10.27
0.700	9.505	8.128	9.589	10.33
0.800	9.893	8.486	10.09	10.93
0.900	10.31	8.867	10.74	11.68
1.000	10.75	9.272	10.91	11.83
1.100	11.21	9.703	11.67	12.68
1.200	11.71	10.16	11.64	12.64
1.300	12.25	10.66	12.39	13.55
1.400	12.82	11.18	12.58	13.72
1.500	13.43	11.75	13.20	14.43
1.600	14.09	12.35	14.20	15.62
1.700	14.79	13.00	14.82	16.31
1.800	15.55	13.71	15.34	16.87
1.900	16.37	14.46	16.03	17.72
2.000	17.26	15.28	17.30	19.13
2.100	18.22	16.17	17.62	19.60
2.200	19.26	17.14	18.63	20.66
2.300	20.40	18.19	19.74	22.06
2.400	21.64	19.33	21.20	23.68
2.500	23.00	20.59	22.11	24.81
2.600	24.48	21.97	23.88	26.92
2.700	26.12	23.48	24.86	28.09
2.800	27.93	25.16	26.49	29.95
2.900	29.93	27.01	28.66	32.69
3.000	32.15	29.07	30.61	34.99
3.100	34.64	31.38	32.77	37.65
3.200	37.42	33.96	35.27	40.75
3.300	40.55	36.87	38.03	44.09
3.400	44.09	40.16	41.48	48.39
3.500	48.11	43.90	44.66	52.40
3.600	52.71	48.19	49.25	58.24
3.700	58.01	53.12	53.90	64.19
3.800	64.14	58.85	59.57	71.51
3.900	71.30	65.54	65.68	79.57
4.000	79.74	73.42	73.48	89.84
4.100	89.76	82.81	82.65	102.2
4.200	101.8	94.10	93.52	116.9
4.300	116.4	107.9	107.3	136.0
4.400	134.5	124.8	122.6	157.4
4.500	157.0	146.1	145.1	188.2
4.600	185.8	173.4	170.7	222.4
4.700	223.3	209.0	206.0	261.7
4.800	273.5	256.8	253.1	298.5
4.900	342.6	323.0	319.8	328.5

TABLE III
TABULATED DATA FOR THE CHANGE IN CO-ENERGY FOR ALL CHANGES IN POSITION, GIVEN TO 4 SIGNIFICANT FIGURES.

Fig. 10. Force versus displacement for the four methods of calculating inductance. Tabulated values evident in table III.